Role of Ser11 in the stabilization of the structure of Ochrobactrum anthropi glutathione transferase

Luca Federici, Michele Masulli, Daniele Bonivento, Adele Di Matteo, Stefano Gianni, Bartolo Favaloro, Carmine Di Ilio, Nerino Allocati

Biochemical Journal Immediate Publication. Published on 16 Jan 2007 as manuscript BJ20061707

Role of Ser11 in the stabilization of the structure of *Ochrobactrum anthropi* glutathione transferase

Luca FEDERICI*†, Michele MASULLI†, Daniele BONIVENTO‡, Adele DI MATTEO‡, Stefano GIANNI§, Bartolo FAVALORO*†, Carmine DI ILIO*† and Nerino ALLOCATI†[1]

**Ce.S.I. Centro Studi sull'Invecchiamento, Fondazione Università "G.d'Annunzio" and †Dipartimento di Scienze Biomediche, Universita' di Chieti "G. d'Annunzio", Via dei Vestini 31, 66013 Chieti, Italy. ‡Dipartimento di Scienze Biochimiche, and §Istituto di Biologia e Patologia Molecolari del Consiglio Nazionale delle Ricerche, Università di Roma "La Sapienza," Piazzale A. Moro 5, 00185 Rome, Italy.*

Short title: Crystal structure of GST from *Ochrobactrum anthropi*

Abbreviations used: *GSH, glutathione; CDNB, 1-chloro-2,4-dinitrobenzene; GdnHCl, guanidine hydrochloride; GST, glutathione transferase; OaGST, Ochrobactrum anthropi glutathione transferase*.

Correspondence to: n.allocati@dsb.unich.it

SYNOPSIS

Glutathione transferases (GSTs) are a multifunctional group of enzymes, widely distributed and involved in cellular detoxification processes. In the xenobiotic degrading bacterium *Ochrobactrum anthropi*, GST is overexpressed in the presence of toxic concentrations of aromatic compounds such as 4-chlorophenol and atrazine. We have determined the crystal structure of the GST from *O. anthropi* (OaGST) in complex with GSH. Like other bacterial GSTs, OaGST belongs to the beta class and shows a similar binding pocket for GSH. However, in contrast with the structure of *Proteus mirabilis* GST, GSH is not covalently bound to Cys^{10} but is present in the thiolate form. In our investigation of the structural basis for GSH stabilization we have identified a conserved network of hydrogen-bond interactions, mediated by the presence of a structural water molecule that links Ser^{11} to Glu^{198}. Partial disruption of this network, by mutagenesis of Ser^{11} to Ala, increases the K_m for GSH by 15 fold and decreases the catalytic efficiency by 4 fold, even though Ser^{11} is not involved in GSH binding. Thermal and chemical induced unfolding studies point to a global effect of the mutation on the stability of the protein and to a central role of these residues in zippering the terminal helix of the C-terminal domain to the starting helix of the N-terminal domain.

Key words: *Ochrobactrum anthropi*; bacterial GST; G-site; unfolding; crystallography; circular dichroism

INTRODUCTION

Glutathione transferases (GSTs; EC 2.5.1.18) are a family of multifunctional enzymes involved in cell detoxification from xenobiotic compounds [1-5]. The classical reaction catalyzed by GSTs is the conjugation of glutathione (GSH) to hydrophobic electrophilic compounds, which generates products that are more easily expelled from the cell [1-4]. Together with this activity, GSTs also show peroxidase and isomerase activities and are capable of binding several substrates non-catalytically [1-4]. GSTs are divided into at least three major families of proteins, namely cytosolic, mitochondrial and microsomal GSTs [5]. The cytosolic GSTs have been sub-grouped into several divergent classes on the basis of sequence identity, substrate specificity and type of catalyzed reactions [5, 6]. Despite interclass sequence identity being often less than 20%, all cytosolic GSTs are dimeric proteins showing a very conserved fold consisting of two domains: a N-terminal thioredoxin-like domain and C-terminal all helical domain [3, 6]. Two binding sites are located at the domains' interface, the G-site that accommodates GSH and the H-site where the hydrophobic electrophiles bind [3, 6].

Several GSTs of bacterial origin have been grouped into their own class (known as beta class) and are characterized by a relatively poor conjugation activity as compared to mammalian GSTs [7]. They are capable of binding several antibiotics including tetracycline and rifamycin, show some differences in their dimeric organisation as compared to mammalian GSTs and perform glutaredoxin-like activity [8-10]. Beta class GSTs are characterized by the presence of a cysteine in the G-site [9]. Notably GSH forms a mixed disulphide with Cys^{10} in the structure of GST from *Proteus mirabilis* (PmGST) while it is present in the thiolate form in the structure of GST from *Burkholderia xenovorans* (BxGST) [10, 11]. Cys^{10} was demonstrated to play a role in the glutaredoxin-like reaction catalyzed by PmGST [10], while its mutation to alanine did not perturb the classical conjugation activity of PmGST, in a fashion similar to the substitution of the catalytic tyrosine or serine of other GST classes, leaving the structural basis of GSH thiolate stabilization in beta class GSTs unclear [12].

Ochrobactrum anthropi is a xenobiotics-degrading bacterium that is able to proliferate in the presence of highly toxic compounds such as phenol, 4-chlorophenol and atrazine and to use them as a carbon source [13, 14]. The overexpression of the

gene encoding a functional GST (OaGST), mainly localized in the periplasm [15], is achieved by the treatment with such aromatic compounds pointing to the hypothesis that this enzyme serves in cellular detoxification processes [14, 16].

In this work we have determined the crystal structure of OaGST in complex with GSH and analyzed similarities and differences with other bacterial GSTs. We identify a network of hydrogen-bond interactions, conserved in all beta class GSTs, that zippers the terminal helix of the C-terminal domain to the starting helix of the thioredoxin-like domain. In order to characterize the role of this network in the G-site and overall protein stabilization we have partially disrupted it by mutating Ser^{11} to Ala. Our results demonstrate that Ser^{11} plays a crucial role in both the stability and functionality of OaGST.

MATERIAL AND METHODS

Expression and purification of wild-type and mutant OaGST enzymes

The recombinant OaGST and S11A mutant enzymes were expressed in *Escherichia coli* XL1-Blue strains as previously described [17]. Briefly, *E. coli* cells were grown overnight at 37°C in Luria-Bertani (LB) medium [18], diluted 1:10 and grown in fresh LB medium until the A_{550} reached 0.4. To induce gene transcription, IPTG (isopropyl-β-D-thiogalactopyranoside) (Sigma-Aldrich, Milano, Italy) was added to a final concentration of 1 mM and the incubation time was prolonged for a further 16 h after switching the temperature to 25°C.

The bacterial cells were collected by centrifugation, washed twice and resuspended in 0.025 M imidazole-HCl, pH 7.4 (buffer A) containing 2 mM dithiothreitol and disrupted by sonication in the cold. The particulate material was removed by centrifugation and the resulting supernatant was subjected to chromatofocusing on a column (i.d. 1.0 cm, height 50 cm) containing polybuffer exchanger PBE 94 (Amersham) equilibrated with buffer A. The column was eluted with polybuffer 74 (Amersham) diluted 1:8, pH 4.0 (flow rate 35 ml/h, fraction volume 2 ml). The peak of activity thus separated was concentrated and dialysed against 10 mM Tris/HCl, pH 7.5 (buffer B), by ultrafiltration in an Amicon apparatus. Concentrated enzyme was further purified by anion-exchange chromatography with a DEAE column (i.d. 1.5 cm, height 11 cm; Bio-Rad Laboratories, Milano, Italy) equilibrated with buffer B.

The enzyme was eluted with a 100 ml linear gradient of 0-0.6 M KCl in buffer B (flow rate 0.5 ml/min, fraction volume 1 ml). The peak containing GST activity was pooled, concentrated, dialysed against 10 mM potassium phosphate buffer (pH 7.0) containing 1 mM EDTA by ultrafiltration and subjected to further analyses. SDS/PAGE in discontinuous slab gel was performed by the method of Laemmli [19]. Protein concentration was determined by the method of Bradford [20] with γ-globulin as standard.

Crystallization and data collection

Wild-type OaGST was extensively dialyzed against water and concentrated up to 5 mg/ml. Prior to crystallization trials, GSH 10 mM was added to the protein sample. Crystals were obtained by the hanging drop vapour diffusion method using the following protocol: 1 μl of protein sample was mixed in a cover slip with 1 μl of a reservoir solution containing 2.0 M ammonium sulphate, Tris pH 7.0 100 mM and 200 mM Li_2SO_4. The cover slip was sealed on a well containing 1.0 ml of the same reservoir solution and equilibrated at 295 K. Crystals appeared after three days and reached a final size of 0.1x0.1x0.2 mm. The addition of GSH was found to be indispensable for crystal growth. The same or other crystallization conditions failed to produce crystals of the S11A enzyme.

Best data for wild-type OaGST were collected at the ID14-4 beamline of ESRF synchrotron source (Grenoble) equipped with an Oxford cryostream system set at 100 K. Before freezing, crystals were cryoprotected by pouring them in a solution identical to the mother liquor plus 25% glycerol. Complete data were collected to the resolution of 2.1 Å. Data were processed and scaled using DENZO and SCALEPACK, respectively [21]. Crystals belong to the space group $P6_122$. Unit cell dimensions together with statistics about the data processing are summarized in Table 1.

Structure solution and refinement

The structure of OaGST was determined by Molecular Replacement using as a search model the structure of *E. coli* GST monomer (pdb code 1A0F), including all side chains but with the exclusion of the glutathione sulphoxide ligand. The program MOLREP from the CCP4 suite was used [22]. The optimal solution yielded a single

monomer in the asymmetric unit, in accordance to Matthews coefficient calculations, and the physiological dimer was correctly generated by crystallographic symmetry. With this asymmetric unit composition, the solvent content of the crystal is 49%. This solution was initially refined using rigid body minimization and simulated annealing as implemented in the program CNS [23]. At this stage electron density maps were visually inspected and clear electron density for GSH was observed. Model building and refinement were carried out iteratively using COOT [24], to visualize the maps and adjust the model, and restrained refinement as implemented in REFMAC5 [25]. An area of positive electron density in the difference Fo-Fc map, contoured at 3.0 σ, was found at the dimer interface in exact correspondence with the symmetry axis. Given its shape and the crystallization conditions, this area was interpreted by adding a sulphate ion to the model. The final model was refined to a R-factor of 18.7% and a Rfree of 23.2 % and contains all 201 residues of the protein, one sulphate ion and 96 water molecules. The final quality of the model is excellent as judged using PROCHECK [26]. Only Gln^{65} has unfavourable stereochemistry according to Ramachandran calculations: this residue is implicated in GSH binding and shows the same stereochemistry in all GSTs determined so far. Notably, Tyr^{86} was found to assume two different conformational states in the monomers forming the physiological dimer. Since the dimer is obtained through crystallographic symmetry, Tyr^{86} was modelled in two configurations with halved occupancies. Statistics relative to the refinement and the quality of the model are shown in Table 1.

Structural superpositions were performed using the program COOT. Contact maps where calculated using the CONTACT MAP ANALYSIS algorithm as implemented in the SPACE server (http://ligin.weizmann.ac.il/cma). Figures 1 and 3 were prepared using PyMOL [27].

The coordinates and structure factors were deposited within the Protein Data Bank and the accession code is 2NTO.

Enzyme activity

GST activity with CDNB (1-chloro-2,4-dinitrobenzene) was assayed at 25°C according to the method of Habig and Jakoby [28]. For the enzyme kinetic determinations either CDNB or GSH were held constant at 1 and 5 mM respectively, whilst the concentration of the other substrate was varied (0.1–5 mM for GSH and

0.1–1.6 mM for CDNB). Each initial velocity was measured at least in triplicate. The KaleidaGraph Software package (Synergy Software, Reading, PA, U.S.A.) was used to estimate the Michaelis constant (K_m) and V_{max} values by non-linear regression analysis using the Michaelis-Menten equation.

The dependence of k_{cat}/K_m on pH was determined by using the following buffers (0.1 M) at the indicated pH values: Bis-Tris/HCl, from 5.0 to 7.0; and Tris/HCl, from 7.2 to 9.0. The reactions were carried out using saturating GSH (5 mM) and variable CDNB concentrations. The pK_a values were obtained by fitting the data to the equation: $\log(k_{cat}/K_m) = \log[C/(1+[H^+]/K_a)]$ where C is the upper limit of k_{cat}/K_m at high pH [29].

Measurements of enzyme activity (0.7 μM) as a function of temperature were carried out by incubating the samples at each temperature for 15 min. GST activity was determined at the end of the incubation.

Unfolding studies

To study the dependence of enzyme activity on GdnHCl concentration, wild-type and mutant GST (7 μM) were first incubated for 30 min at 25 °C in 0.1 M potassium phosphate buffer (pH 6.5) containing 1 mM EDTA with 0-4 M GdnHCl. At the end of incubation, each sample was assayed for remaining GST activity in 1 ml of final volume but including the same concentration of GdnHCl as used in the incubation.

Equilibrium thermal denaturations were followed on a JASCO circular dichroism (CD) spectrophotometer using a 0.1 cm quartz cuvette (Hellma). Protein concentration was 5 μM. Data for wild type and S11A enzymes were fitted using the equation:

$$y_{obs} = y_N + y_D \frac{e^a}{1+e^a}$$

$$\text{with } a = \frac{-\Delta H_{Tm} - (1-\frac{T}{T_m}) - \Delta c_p (T_m - T) + \Delta c_p (RT \cdot \log(\frac{T}{T_m}))}{RT}$$

where y_N and y_D represent the CD signals of the native and denatured state, respectively; T_m is the melting temperature; ΔH_{Tm} is the change in enthalpy upon

denaturation at the melting temperature and the Δc_p is the heat capacity change upon unfolding.

In the analysis, the S11A enzyme data were cut at the temperature of 328 K because at this temperature the protein grossly precipitates.

GdnHCl-induced equilibrium denaturations were performed at 298 K recording CD spectra in the interval 215-230 nm. GdnHCl concentration was progressively increased by 0.2 M, from 0 to 4.6 M, and the spectra recorded using a 1.0 cm quartz cuvette (Hellma) and a protein concentration of 1 μM. Assuming a standard two-state model, the GdnHCl-induced denaturation transition for the wild-type enzyme was fitted to the equation:

$$\Delta G_d = \Delta G^0 - m_{D\text{-}N} D$$

where ΔG^0 is the free energy of folding in water and ΔG_d at a concentration D of denaturant, m_{D-N} is the slope of the transition (proportional to the increase in solvent-accessible surface area on going from the native to the denatured state). An equation that takes into account the pre- and post-transition baselines was used to fit the observed unfolding transition [30].

RESULTS AND DISCUSSION

Overall structure and comparison with beta class GSTs

The structure of OaGST was determined by molecular replacement using the structure of *Escherichia coli* GST (EcGST) as a search model [31]. One monomer of OaGST is found in the asymmetric unit and the physiological dimer is obtained through crystallographic symmetry (Figure 1A). Statistics about data collection and refinement are listed in Table 1.

OaGST displays the typical overall fold of this super-family of enzymes and is composed by two domains: an N-terminal thioredoxin-like domain (residues 1-76) and a C-terminal α-helical domain (residues 89-201), connected by a linker region. Like other bacterial GSTs, OaGST may be classified as belonging to the beta class. A structure-based comparison with the other three GSTs of known structure belonging to this class, PmGST, EcGST and the recently solved BxGST [11], reveals relatively

high sequence identities, i.e. 34%, 39% and 46% respectively. This is reflected in the rms deviations of equivalent Cαs that are 1.488 Å for OaGST-PmGST, 1.38 Å for OaGST-EcGST and 1.33 Å for OaGST-BxGST. These deviations are smaller than those obtained by comparing OaGST with GSTs representative of other classes. In this case rms deviations range from 1.85 Å for the superposition with the delta class GST from *Anopheles gambiae* to 2.67 Å for the superposition with the murine pi class GST. Nevertheless these numbers highlight that the overall GST fold is remarkably well conserved from bacteria to mammals, despite very low inter-class sequence identities.

A peculiarity of beta class GSTs is that their dimer interface is mainly polar and close-packed and differs from the more open and hydrophobic V-shaped interface observed in other classes. The relative orientation of the monomers in the beta-class GST dimers is very well conserved as observed by superposing the OaGST dimer with the PmGST, EcGST and BxGST dimers (Figure 1B). Rms deviations for these superpositions are 1.614 Å, 1.418 Å and 1.54 Å, respectively. These values are very close to those obtained by superposing the monomers alone. Interestingly, such a remarkable conservation in the dimer architecture is achieved through a set of interactions that are only partially conserved. This is shown in Figure 2 where inter-chain contact maps for beta class GSTs are represented. For instance, a number of contacts between residues belonging to the C-terminal domain of both monomers in PmGST and EcGST (lower right in the contact maps) are not conserved in OaGST and partially in BxGST. Conversely in OaGST, a number of contacts between the N-terminal domain of one monomer and the C-terminal domain of the other monomer are not conserved in the other structures (lower left or upper right in the contact maps). Many other differences are also visible throughout the contact maps that provide a fingerprint for each dimer interface. This analysis suggests that, after divergence among the different bacteria, evolution was oriented toward the conservation of the relative orientation of the monomers in the dimers rather than to preserve the chemical nature of the interface.

The G-site

In the structure of OaGST, GSH is stabilized through a number of ionic and H-bond interactions with several residues including Lys^{35}, Val^{52} through its peptide carbonyl and amide groups, Asn^{66} and Gln^{65}. Similarly to other beta class GSTs, GSH bound to

a monomer is hydrogen-bonded to a residue (Asp^{103}) of the other monomer and contributes to the stabilization of the dimer interface in the ligand-bound form. An interesting difference with PmGST is that in the structure of OaGST we do not observe a mixed-disulphide bond between GSH and Cys^{10} (Figure 3). This is also true for the structure of BxGST cocrystallized with GSH [11], while the structure of EcGST was obtained in the presence of the GSH analogue, glutathione sulphonate [31]. In OaGST, the distance between the GSH and enzyme Cys^{10} cysteinyl groups is 3.11 Å suggesting, together with the shape of the electron density, that the GSH is present in the thiolate form and shares a proton with Cys^{10}. The contribution of G-site residues to the thiolate stabilization has been investigated in PmGST and partly in EcGST. In the PmGST structure, three residues were found to be at hydrogen bond distance from the GSH sulphur, namely Cys^{10}, Ser^{9} and His^{106} (in PmGST numbering). Mutation of Cys^{10} to Ala in both PmGST and EcGST did not affect the conjugating activities of these enzymes but caused an increase in the GSH pK_a [10, 32]. Mutation of Ser^{9} to Ala in PmGST caused a moderate loss in specific acitvity but no variation in the pK_a [12]. Finally, mutation of His^{106} to Ala in PmGST caused a dramatic effect to the catalytic activity but only a moderate shift to the GSH pK_a (from 6.4 to 6.7) [33]. By observing the G-site conformation, we note that in OaGST, as well as in BxGST, the topological position corresponding to the PmGST Ser9 is occupied by an alanine that cannot contribute to the thiolate stabilization. Moreover, in OaGST, His^{105} occupies a different position from its topologically equivalent His^{106} of PmGST, BxGST and EcGST. This is due to the absence of charge repulsion with the following Lys^{107} that is topologically replaced by an alanine in OaGST. As a consequence, OaGST His^{105} Nε1 and Nε2 side chain nitrogens are at a distance of 4.58 Å and 4.26 Å, respectively, from the GSH sulphur, as compared to an average distance of ~3.3 Å in the other GSTs, and none of them has a favourable geometry to interact with the GSH sulphur. Thus in the OaGST structure two possible contributors to GSH thiolate stabilization are either absent or in an unfavourable position. Nevertheless, the thiolate stabilization achieved in OaGST is more effective than in PmGST since the pK_a value for GSH in OaGST is 5.96 (Table 2) while in PmGST is 6.4 [10]. Thus it seems plausible to hypothesize that, in OaGST, Cys^{10} plays an important role in both the stabilization of the GSH thiolate and in defining the conjugation activity.

Cys[10] was also found to be crucial for the glutaredoxin-like activity of PmGST [10]. This enzyme is always recovered in the oxidized state after purification, with Cys[10] covalently linked to GSH in a mixed disulphide [9]. Interestingly this is not the case for both OaGST and BxGST that are purified and crystallized in the reduced state. As we have noted before the main difference at the G-site between PmGST and OaGST/BxGST is the presence in the former of a serine at position 9, establishing a H-bond interaction with the GSH sulphur, that is replaced by an alanine in OaGST, BxGST and EcGST. A possible role of PmGST Ser[9] in defining the increased tendency of this enzyme towards the formation of a mixed disulphide as compared to the other beta class GSTs may thus be hypothesized but remains to be established.

Mutation of Ser[11] affects the enzyme activity and G-site stability

By analyzing a sequence alignment of all bacterial GSTs available in the database (data not shown) we observed that, together with Cys[10], Ser[11] is also completely conserved. Mutation of Ser[11] to Ala resulted in a marked loss in activity [17]. The position of this residue in the structure of OaGST attracted our attention since Ser[11] is the first residue of helix 1 and its side chain is not part of the G-site but it points to the opposite direction with respect to Cys[10] side chain (Figure 3). The distance between the Ser[11] hydroxyl group and the GSH sulphur is 6.43 Å, which excludes a direct role in GSH binding and stabilization. A closer analysis of the structure highlights the presence of a network of H-bond interactions that are conserved in all beta-class GSTs (Figure 3). Three residues take part in this network: Ser[11] is linked to Glu[198] through a water molecule that is hydrogen-bonded to both residues. Glu[198] is in turn also hydrogen-bonded to His[15]. The structural role played by the water molecule is witnessed by its thermal B-factor (23.65 Å^2) that is in the range of main chain atoms B-factors. The effect of the Ser[11] to Ala mutation on enzyme function was tested and the specific activities and kinetic constants with CDNB as a second substrate for wild-type and S11A OaGST are shown in Table 2. The effect of the mutation is exerted mainly at the G-site. The K_m for GSH is considerably increased (by 15-fold) while the k_{cat}/K_m is decreased by 5-fold and the specific activity decreased by 3-fold. Interestingly the k_{cat} is increased by 4-fold. Taken together these data suggest that the mutation considerably lowers the affinity for GSH and the overall efficiency of the enzyme but favours the release of the product once the reaction has taken place. Since

Ser^{11} does not bind the GSH, this might, in a first instance, be ascribed to an increased mobility and/or destabilization of the G-site in the mutated enzyme.

The effect on the CDNB kinetic constants is exerted mainly on the K_m but is less evident in agreement with the observation that this mutation is far from the H-site (Table 2). Interestingly a long-range effect is observed also in the GSH thiolate stabilization with a slight decrease of the pK_a from 5.96 to 5.84.

To investigate a possible effect on the structural stability of the enzyme G-site we also followed the conjugation of CDNB by GSH as a function of temperature and GdnHCl concentration. The thermal stability of the S11A enzyme is compromised: while the wild-type enzyme retains more than 80% of its functionality at 50 °C, the S11A enzyme is already almost inactive at 45 °C (Figure 4A). Accordingly, also the effect of GdnHCl is markedly different for the S11A enzyme as compared to the wild-type (Figure 4B). At [GdnHCl]=0.5 M the S11A enzyme has completely lost its activity while the wild-type enzyme still retains 50% of its functionality.

Global effect of the H-bond network on OaGST stability

Next we wanted to establish if the effect of the mutation on enzyme kinetics might be only ascribed to a local effect on the G-site conformation or rather to a global effect on the enzyme stability. Unfortunately every attempt to crystallize this mutant failed, however CD spectra of the wild-type enzyme and the mutated enzyme in the 205-250 nm interval are completely superimposable (inset in Figure 5) suggesting that the structure of the mutant is native-like in physiological conditions.

Figure 5 shows thermal denaturation of the wild-type and mutated enzymes. While the wild-type and S11A enzymes display similar native baselines, confirming that the mutated enzyme is fully folded in physiological temperature range, the transition to the unfolded species is shifted at lower temperature for the mutated enzyme. This is quantitatively confirmed by fitting the experimental data with a two state model. Our analysis suggests that the T_m for the mutated enzyme is decreased by 7 °C (from 56.68 °C to 49.75 °C) and that the overall destabilization caused by the mutation may be estimated as $\Delta\Delta G$ ~1.8 kcal/mol.

We also followed the denaturation of the enzyme in the presence of increasing amounts of GndHCl. In Figure 6 the denaturation profiles for the wild-type and the mutated enzyme are shown and a different behaviour is observed. Again a clear transition for the mutated enzyme is visible at very low GndHCl concentration where

the wild-type enzyme is still fully folded. A closer investigation of the observed denaturation profiles reveals that, while a simple two-state transition can be assigned to the wild-type data, a more complex denaturation is monitored for the S11A mutant. Such behaviour may be consistent with the accumulation of an unfolding intermediate. Taken together, both chemical and thermal unfolding data clearly suggest that a remarkable destabilization is associated with the S11A mutation, i.e. above 60% of the total free energy of the enzyme, the overall stability of the wild-type protein being about 3 kcal/mol.

In this work we have structurally and functionally characterized the GST from *O. anthropi*, a xenobiotics degrading bacterium capable of growing in the presence of highly toxic compounds such as 4-chlorophenol and atrazine. On the basis of its structural similarity with previously characterized GSTs, OaGST may be classified as belonging to the beta class.

Analyzing the structure of OaGST, we have identified a previously unrecognized network of hydrogen bonds, located at the boundaries of the G-site, but distinct from it, that links the first helix of the N-terminal thioredoxin-like domain to the terminal helix of the C-terminal domain. We have shown that the single mutation S11A dramatically alters the catalytic capabilities of the enzyme towards the model substrate CDNB. This is likely the result of the crucial role played by this network in stabilizing the overall fold of the protein, as inferred from chemical and temperature induced unfolding studies. Since this H-bond network is conserved in beta class GSTs but not in GSTs belonging to other classes we conclude that, within the framework of the very conserved GST fold, evolution found different solutions to achieve structural stabilization in the various GST classes.

ACKNOWLEDGEMENTS

We thank the beamline scientists at the ESRF (Grenoble, France) for setting up the experimental beamline for x-ray diffraction. This work was partially supported by grants from Ministero dell'Universita' e della Ricerca.

REFERENCES

1 Hayes, J. D. and Pulford, D. J. (1995) The glutathione S-transferase supergene family: regulation of GST and the contribution of the isoenzymes to cancer chemoprotection and drug resistance. Crit. Rev. Biochem. Mol. Biol. **30**, 445-600

2 Hayes, J. D. and McLellan, L. I. (1999) Glutathione and glutathione-dependent enzymes represent a co-ordinately regulated defence against oxidative stress. Free Rad. Res. **31**, 273-300

3 Armstrong, R. N. (1997) Structure, catalytic mechanism, and evolution of the glutathione transferases. Chem. Res. Toxicol. **10**, 2-18

4 Mannervik, B. and Danielson, U. H. (1988) Glutathione transferases: structure and catalytic activity. Crit. Rev. Biochem. Mol. Biol. **23**, 283-337

5 Hayes, J. D., Flanagan, J. U. and Jowsey, I. R. (2005) Glutathione Transferases. Annu. Rev. Pharmacol. Toxicol. **45**, 51-88

6 Sheehan, D., Meade, G., Foley, V. M. and Dowd, C. A. (2001) Structure, function and evolution of glutathione transferases: implications for classification of non-mammalian members of an ancient enzyme superfamily. Biochem. J. **360**, 1-16

7 Di Ilio, C., Aceto, A., Piccolomini, R., Allocati, N., Faraone, A., Cellini, L., Ravagnan, G. and Federici, G. (1988) Purification and characterization of three forms of glutathione transferase from *Proteus mirabilis*. Biochem. J. **255**, 971-975

8 Perito, B., Allocati, N., Casalone, E., Masulli, M., Dragani, B., Polsinelli, M., Aceto, A. and Di Ilio, C. (1996) Molecular cloning and overexpression of a glutathione transferase gene from *Proteus mirabilis.* Biochem. J. **318**, 157-162

9 Rossjohn, J., Polekhina, G., Feil, S. C., Allocati, N., Masulli, M., Di Ilio, C. and

Parker, M. W. (1998) A mixed disulfide bond in bacterial glutathione transferase: functional and evolutionary implications. Structure **6**, 721-73425

10 Caccuri, A. M., Antonini, G., Allocati, N., Di Ilio, C., De Maria, F., Innocenti, F., Parker, M. W., Masulli, M., Lo Bello, M., Turella, P., Federici, G. and Ricci, G. (2002) GSTB1-1 from *Proteus mirabilis*: a snapshot of an enzyme in the evolutionary pathway from a redox enzyme to a conjugating enzyme. J. Biol. Chem. **277**, 18777-18784

11 Tocheva, E.I., Fortin, P.D., Eltis, L.D., Murphy, M.E.P. (2006) Structures of ternary complexes of BphK, a bacterial glutathione S-transferase that reductively dechlorinates polychlorinated biphenyl metabolites. J Biol Chem. **281**, 30933-40.

12 Casalone, E., Allocati, N., Ceccarelli, I., Masulli, M., Rossjohn, J., Parker, M. W. and Di Ilio, C. (1998) Site-directed mutagenesis of the *Proteus mirabilis* glutathione transferase B1-1 G-site. FEBS Lett. **423**, 122-124

13 Laura, D., De Socio, G., Frassanito, R. and Rotilio, D. (1996) Effects of atrazine on *Ochrobactrum anthropi* membrane fatty acids. Appl. Environ. Microbiol. **62**, 2644-2646

14 Favaloro, B., Tamburro, A., Trofino, M.A., Bologna, L., Rotilio, D. and Heipieper, H.J. (2000) Modulation of the glutathione S-transferase in *Ochrobactrum anthropi*: function of xenobiotic substrates and other forms of stress. Biochem. J. **346**, 553–559

15 Tamburro, A., Robuffo, I., Heipieper, H.J., Allocati, N., Rotilio, D., Di Ilio, C. and Favaloro, B. (2004) Expression of glutathione S-transferase and peptide methionine sulphoxide reductase in *Ochrobactrum anthropi* is correlated to the production of reactive oxygen species caused by aromatic substrates. FEMS Microbiol. Lett. **241**, 151–156

16 Tamburro, A., Allocati, N., Masulli, M., Rotilio, D., DiIlio, C. and Favaloro, B. (2001) Bacterial peptide methionine sulphoxide reductase: co-induction with

glutathione S-transferase during chemical stress conditions. Biochem. J. **360**, 675–681

17 Favaloro, B., Tamburro, A., Angelucci, S., De Luca, A., Melino, S., Di Ilio, C., and Rotilio, D. (1998) Molecular cloning, expression and site-directed mutagenesis of glutathione S-transferase from *Ochrobactrum anthropi*. Biochem. J. **335**, 573-579

18 Sambrook, J. and Russell, D. W. (2001) Molecular cloning: A Laboratory Manual, 3rd edn, Cold Spring Harbor Laboratory, Cold Spring Harbor, N.Y.

19 Laemmli, U.K. (1970) Cleavage of structural proteins during the assembly of the head of bacteriophage T4. Nature (London) **227**, 680-685

20 Bradford, M.M. (1976) A rapid and sensitive method for the quantitation of microgram quantities of protein utilizing the principle of protein-dye binding. Anal. Biochem. **72**, 248-254

21 Otwinowski, Z. and Minor, W. (1997) Processing of X-ray diffraction data collected in oscillation mode. Methods Enzymol. **276**, 307–326

22 Vagin, A., and Teplyakov, A. (2000) An approach to multi-copy search in molecular replacement. Acta Crystallogr D Biol Crystallogr. **56**, 1622-1624

23 Brunger, A. T., Adams, P. D., Clore, G. M., DeLano, W. L., Gros, P., Grosse-Kunstleve, R. W., Jiang, J. S., Kuszewski, J., Nilges, M., Pannu, N. S., Read, R. J., Rice, L. M., Simonson, T., and Warren, G. L. (1998) Crystallography & NMR system: A new software suite for macromolecular structure determination. Acta Crystallogr. D Biol. Crystallogr. **54**, 905-921

24 Emsley, P., and Cowtan, K. (2004) Coot: model-building tools for molecular graphics. Acta Crystallogr. Sect. D Biol. Crystallogr. **60**, 2126–2132

25 Murshudov, G. N., Vagin, A. and Dodson, E. J. (1997) Refinement of Macromolecular Structures by the Maximum-Likelihood Method. Acta Crystallogr. Sect. D Biol. Crystallogr. **53**, 240–255

26 Laskowsky, R. A., MacArthur, M. W., Moss, D. S. and Thornton, J. R. (1993) PROCHECK- A program to check the stereochemical quality of protein structures. J. Appl. Crystallogr. **26**, 283-291

27 DeLano, W. L. (2002) The PyMOL Molecular Graphics System. DeLano Scientific, San Carlos, CA, USA

28 Habig, W. H., and Jakoby, W. B. (1981) Assay for differentiation of glutathione S-transferases. Methods Enzymol. **77**, 398-405

29 Liu, S., Zhang, P., Ji, X., Johnson, W. W., Gilliland, G. L. and Armstrong, R. N. (1992) Contribution of tyrosine 6 to the catalytic mechanism of isoenzyme 3-3 of glutathione S-transferase. J. Biol. Chem. **267,** 4296-4299

30 Santoro, M.M. and Bolen, D.W. (1988) A test of the linear extrapolation of unfolding free energy changes over an extended denaturant concentration range. Biochemistry **27**, 8063–8068.

31 Nishida, M., Harada, S., Noguchi, S., Satow, Y., Inoue, H., and Takahashi, K. Three-dimensional structure of *Escherichia coli* glutathione S-transferase complexed with glutathione sulfonate: catalytic roles of Cys10 and His106. J Mol Biol **281**, 135-147.

32 Inoue H, Nishida M and Takahashi K (2000). Effect of Cys10 mutation to Ala in glutathione transferase from *Escherichia coli*. J. Organ. Chem. **611**, 593-595.

33 Allocati N, Casalone E, Masulli M, Polekhina G, Rossjohn J, Parker MW, Di Ilio C. (2000) Evaluation of the role of two conserved active-site residues in beta class glutathione S-transferases. Biochem J. **351**, 341-346.

FIGURE LEGENDS

Figure 1. A) Ribbon representation of the physiological dimer of OaGST. Bound GSH molecules are shown in sticks. A sulphate ion, found at the interface between monomers, exactly marks the position of the crystallographic 2-fold axis.
B) Structural superposition of GST dimers belonging to the beta class: OaGST (light blue), PmGST (magenta), EcGST (orange) and BxGST (green).

Figure 2. Contact maps for beta class GSTs. Interactions between residues belonging to different monomers in the dimers are shown as squares. Several differences are observed throughout the maps, even though the orientations of the monomers in the various GSTs dimers are conserved.

Figure 3. Close up view of OaGST in the GSH surroundings. Cys^{10} is not covalently linked to the GSH. Residue Ser^{11} is oriented in the opposite direction and interacts with Glu^{198} *via* a structural water molecule. Glu^{198} is also hydrogen-bonded to His^{15}. These residues are conserved in beta class GSTs.

Figure 4. A) OaGST residual activity with CDNB as a function of temperature and B) OaGST residual activity with CDNB as a function of increasing concentrations of GdnHCl. Wild-type enzyme (●). S11A enzyme (□).

Figure 5. Thermal melt of OaGST followed by circular dichroism. Data were fitted with a two-state model. Straight line represents wild-type OaGST data; dashed line represents S11A OaGST data. The overall destabilization caused by this single point mutation is estimated to be 1.8 kcal mol^{-1}. Inset shows CD spectra for wild-type (straight line) and S11A (dashed line) in the interval 200-250 nm.

Figure 6. GdnHCl-induced equilibrium denaturation of OaGST followed by circular dichroism. Wild type data are represented with filled circles, S11A data are shown with empty circles. Wild-type data were fitted with a two-state model. This model could not be applied satisfactorily to the S11A data, due to the appearance of an unfolding intermediate. Overall stability of the protein is estimated to be 2.86 kcal/mol.

Table 1 Summary of crystallographic data and refinement

Beamline	ESRF ID14-4
Wavelength (Å)	0.934
Resolution (Å)	50.6-2.1
(last shell)	2.18-2.10
R_{merge}	0.070 (0.335)*
Unique reflections	13632
Completeness (%)	99.9 (99.8)
Multiplicity	13.21
I/σ*(I)*	11.8
Cell dimensions	a=b= 58.765 Å c= 212.323Å
Space group	$P6_122$
Refinement	
R (working set)	0.187
R_{free} (test set)	0.232
R.m.s. deviations	
Bond lengths (Å)	0.010
Bond angles (°)	1.307
Ramachandran statistics	
% of residues in most favoured regions	94.8
% of residues in allowed regions	4.7
% of residues in non allowed regions	0.6
Model	
amino acids	1-201 (one monomer in the asymmetric unit)
glutathione	1
water molecules	122
sulphates	1

* Numbers in parentheses refer to the highest resolution shell

Table 2. Specific activity and kinetic constants for OaGST and the S11A mutant with CDNB as second substrate. The values are presented as means ± S.D. for at least three independent determinations.

		GSH			CDNB			
Enzyme	Specific activity (μmol $min^{-1}mg^{-1}$)	K_m (mM)	k_{cat} (s^{-1})	k_{cat}/K_m (mM^{-1} s^{-1})	K_m (mM)	k_{cat} (s^{-1})	k_{cat}/K_m (mM^{-1} s^{-1})	pK_a^{CDNB}
OaGST	5.9±0.43	0.133±0.01	2.36±0.12	17.78	3.094±0.19	16.5±0.82	5.33	5.96±0.17
S11A	2.2±0.15	1.917±0.12	9.23±0.56	4.81	1.187±0.08	14.1±0.49	11.87	5.84±0.22

Biochemical Journal Immediate Publication. Published on 16 Jan 2007 as manuscript BJ20061707

Figure 1

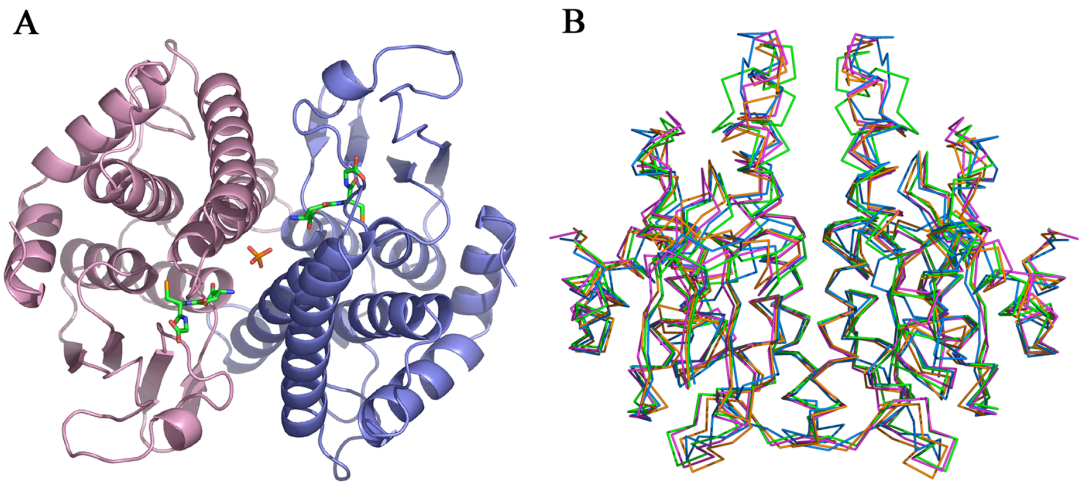

Figure 2

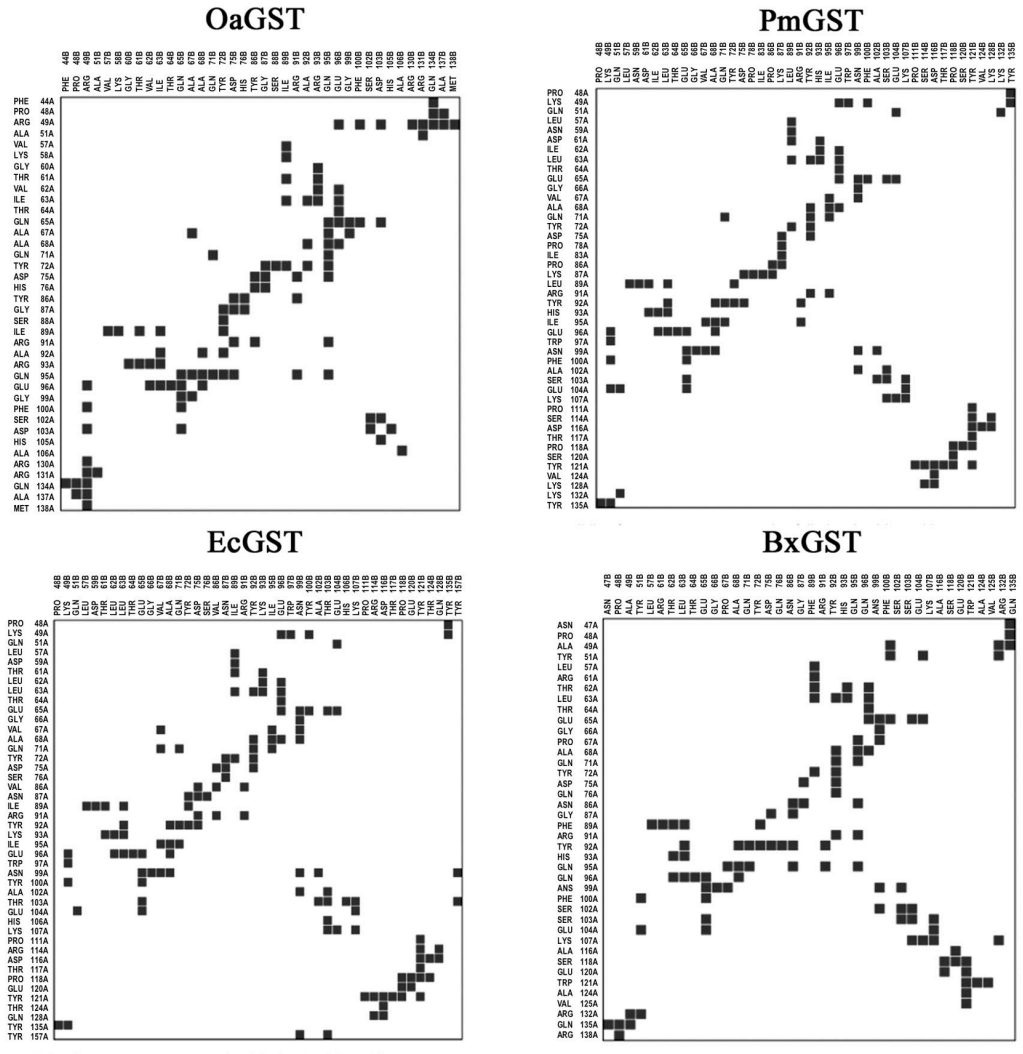

Figure 3

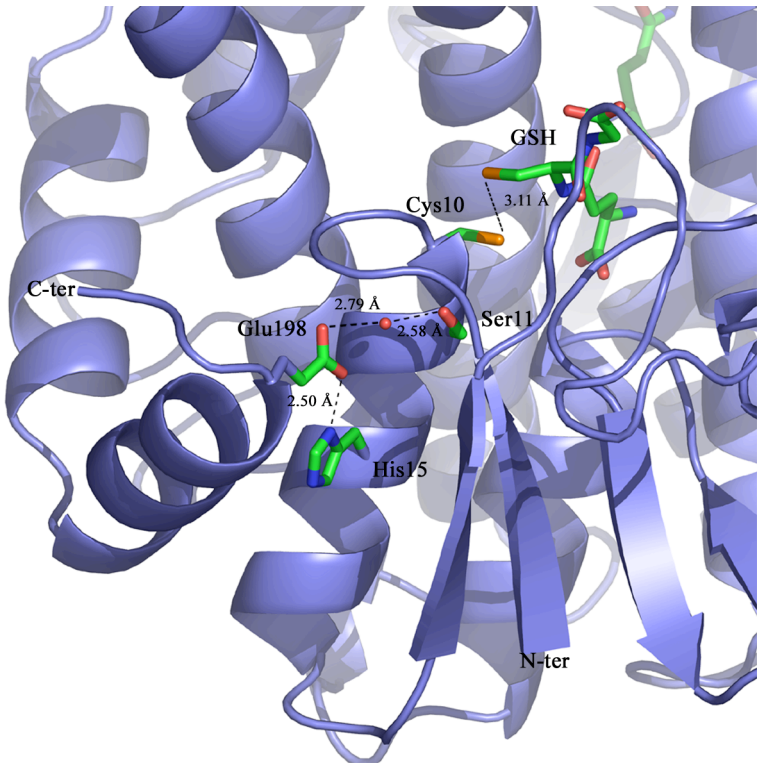

Figure 4

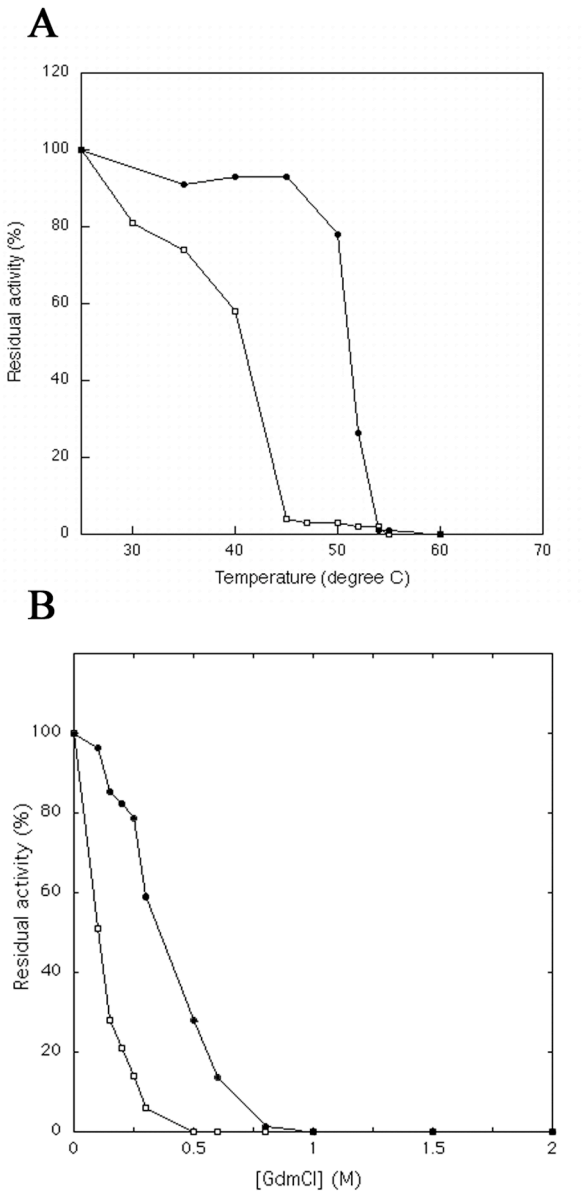

Biochemical Journal Immediate Publication. Published on 16 Jan 2007 as manuscript BJ20061707

Figure 5

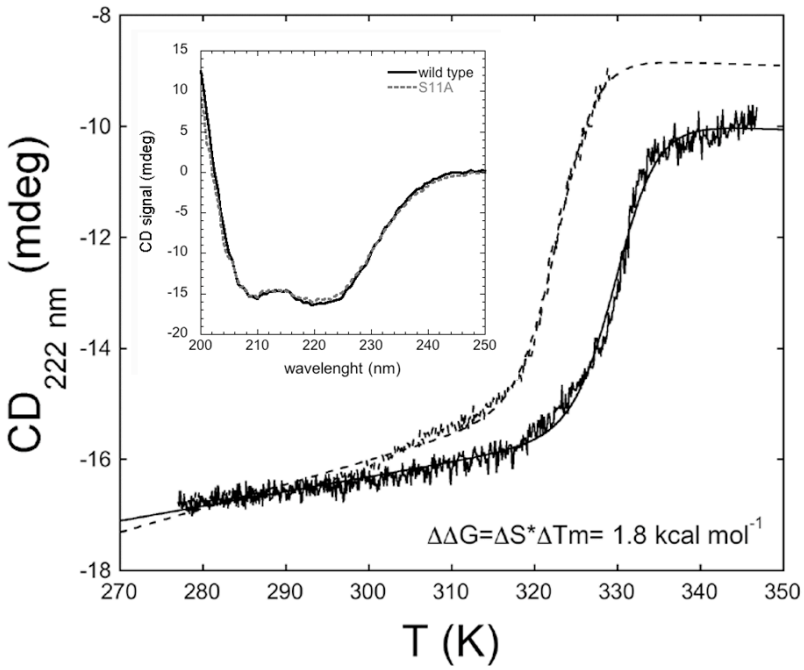

Figure 6